

Decision Feedback Differential Detection for Reconfigurable Intelligent Surfaces

Jiawei Qiu and Harry Leib

Abstract

This work considers a Differential Reflecting Modulation (DRM) scheme for Reconfigurable Intelligent Surfaces (RIS) not requiring channel state information (CSI). When operating over time-varying fading channels, such schemes with Conventional Differential Demodulation (CDD) receivers experience high error floors and performance degradation. To address these issues, we propose a Decision Feedback Differential Detection (DFDD) technique for DRM. We explore the application of DFDD for RIS DRM and conduct extensive Monte-Carlo simulations to analyze performance. Results demonstrate the viability of our DFDD technique across various RIS scenarios and highlight the importance of proper parameter selection to achieve good performance. The DFDD scheme is also compared with uncoded and Differential Space-Time Modulation (DSTM) coded DRM using CDD based receivers. We observe that at low SNR, the DFDD scheme performs almost as well as the DRM with CDD scheme, but worse than the DSTM coded DRM. As the SNR increases however, both CDD-detected systems encounter high error floors while the error rate of DFDD based scheme continues to improve until it reaches a relatively low error floor. It is shown that the chief merits of employing DFDD receivers in such RIS systems is the low error floors they provide over time varying fading channels, albeit at expense of a small increased complexity.

I. INTRODUCTION

The Reconfigurable Intelligent Surface (RIS) technology, also referred to as Intelligent Reflecting Surface (IRS), holds significant potential for facilitating an advantageous wireless communication environment [1]–[6]. An RIS system consists of a large number of passive

Jiawei Qiu was with the Department of Electrical and Computer Eng. McGill University, Montreal QC Canada. He is now with INRS Telecommunications, University of Quebec, Montreal QC Canada.

Harry Leib is with the Department of Electrical and Computer Eng., McGill University, Montreal, QC Canada, Email: harry.leib@mcgill.ca

reflecting units, each capable of altering the incident signals in terms of phase and amplitude. These units are made from electromagnetic material, with size and spacing much smaller than the wavelength. Unlike relays, RIS can be constructed with minimal hardware complexity and cost, employing low-power and low-complexity electronic circuits [7]. The primary characteristic of RIS is its reconfigurability after deployment in a wireless environment, allowing for a programmable and controllable communication environment [8].

Recently, there has been a notable interest in research on RIS communication techniques. A substantial volume of literature has been dedicated to exploring RIS modulation techniques [9]–[14], and channel state information (CSI) [15]–[19]. Alwazani *et al* in [15] introduced an RIS-assisted multi-user multiple-input single-output (MISO) communication system under imperfect CSI, demonstrating the efficiency of this scheme and its high sensitivity to the quality of the estimates. However, to the best of our knowledge, most schemes assume perfect CSI for detection [20]–[23]. Channel estimation in an RIS-based communication system has to consider the transmitter-RIS, RIS-receiver, and direct transmitter-receiver links. Such estimations schemes are complicated due to the absence of baseband signal processing capabilities in RIS units. While efforts have been made to address the challenges of channel estimation in RIS systems [15], [21], [24], [25], CSI acquisition remains a significant and challenging problem, making transmission techniques not requiring CSI attractive..

Noncoherent detection is a demodulation technique that does not require CSI, thereby reducing the complexity of communication systems. Moreover, noncoherent demodulation could be more reliable than coherent demodulation, particularly at low SNR, due to the latter's reliance on CSI which presents challenges to acquire [26]. As a result, RIS-assisted systems employing noncoherent detection techniques have attracted considerable interest [27]–[33]. In [29], Cai *et al* present a noncoherent RIS-assisted joint index keying M -ary differential chaos shift keying scheme. This system enables the receiver to employ noncoherent correlation without the need for CSI, thus reducing system complexity. Simulation results indicate that this technique outperforms existing systems. In [31], an RIS-aided differential chaos shift keying technique is proposed to overcome the limited BER performance gains observed in noncoherent chaotic communications. By deploying RIS near the transmitter antenna, the scheme enhances the SNR of the received signal, significantly improving error performance.

Despite of many advantages of noncoherent demodulation, [34] noted that conventional

differential detection (CDD) for RIS, which a common form of noncoherent detection, results in performance degradation. For scalar communication systems, more advanced noncoherent detection techniques have been introduced to improve performance.. The concept of Decision Feedback Differential Detection (DFDD) was first proposed by [35] and analyzed in [36]. The DFDD technique utilizes feedback from previously detected symbols to establish a demodulation reference, leading to a possible improvement in BER performance over CDD that employs only the previous symbol as a reference. Demodulators based on DFDD have been initially considered for AWGN channels in [35] and later extended to fading channels in [37], [38]. In [37], it was concluded that DFDD employing finite-order feedback filters can significantly reduce the error floor compared to CDD. Due to their effectiveness in scalar transmission systems, DFDD techniques have triggered research into corresponding detection methods for multi-antenna scenarios. In [39], DFDD based structures were applied to unitary-matrix signaling-based DSTM over Multiple-Input Multiple-Output (MIMO) fading channels.

Our paper considers, a DRM scheme from [34] for RIS systems. Different from [29]–[33], this DRM scheme operates on M -ary PSK. Information bits are mapped to both the activation permutations order of the reflecting patterns and the phases of transmitted signals, which facilitate CDD based demodulation, avoiding channel estimation. However, CDD may result in performance loss and error floor over time-varying fading channels for DRM. This motivates to consider a DFDD technique for DRM RIS systems operating over time-varying Rayleigh fading channels. Our work demonstrates that the use of DFDD techniques for such RIS systems lowers significantly the error floors when compared to CDD.

The rest of this paper is organized as follows. In section II, we introduce the system model of the DRM RIS system. The fundamentals of DFDD demodulation, its extension to DRM and performance issues are presented in Section III. Section IV offers a performance comparison between DFDD DRM against uncoded DRM and DRM-DSTM coded schemes employing CDD, since the latter has also error floor reduction capabilities. In our paper we also evaluate the associated computational complexities. Conclusions are drawn in Section V, and Appendix A presents the details of the DFDD prediction coefficients derivation.

II. SYSTEM MODEL AND FUNDAMENTALS OF DFDD-DETECTED DRM

We consider a model for an RIS system employing Differential Reflecting Modulation (DRM) as in [40, Figure 1]. Let $\mathbf{X}[t] \in \mathbb{C}^{K \times K}$ be the information carrying matrix $\mathbf{X}[t] = \mathbf{Z}[t]\mathbf{S}[t]$ where $\mathbf{Z}[t]$ is a $K \times K$ permutation matrix, and $\mathbf{S}[t]$ is a $K \times K$ diagonal matrix of MPSK symbols [40]. The number of information bits that $\mathbf{X}[t]$ carries is shown in [40] to be

$$r = \lfloor \log_2 K! \rfloor + K \log_2 M \quad (1)$$

where M is the MPSK constellation order. Then matrix differential encoding is performed

$$\mathbf{V}[t] = \mathbf{V}[t-1]\mathbf{X}[t], \quad (2)$$

where $\mathbf{V}[t-1]$ is generated in the previous block. The first block in a frame does not convey information, thus $\mathbf{V}[0]$ is set as an identity matrix.

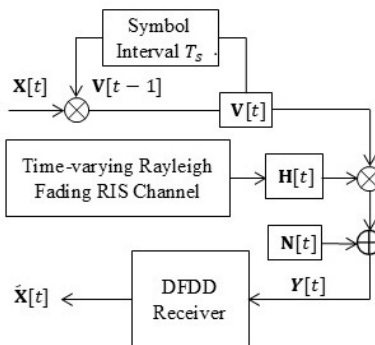


Fig. 1: DFDD-detected DRM encoding structure

The equivalent system to [40, Figure 1] we consider in our present paper aiming at deriving a DFDD receiver for a DRS RIS system can be represented by:

$$\mathbf{Y}[t] = \mathbf{H}[t]\mathbf{V}[t] + \mathbf{N}[t], \quad (3)$$

and it is illustrated in Fig.1. The equivalent channel matrix [40] is $\mathbf{H}[t]$ which is determined by the channels from the transmitter to RIS, from RIS to receiver including RIS reflecting pattern selection, and also by the direct channel from the transmitter to receiver. The additive noise matrix is $\mathbf{N}[t] \in \mathbb{C}^{N_r \times K}$. The channels are represented as zero-mean complex Gaussian processes (time varying Rayleigh fading based on Jakes model). of unity normalized power, and spatially uncorrelated [41]. The autocorrelation function (ACF) of the symbol-rate-sampled fading process is given by $J_0(2\pi f_D m T_s)$ where $J_0(\cdot)$ denotes the zeroth-order

Bessel function of the first kind, and $f_D T_s$ represents the normalized Doppler frequency [41]. At values of $f_D T_s$ used in this work the fading process essentially remains constant over a time interval of duration T_s , hence we assume the absence of intersymbol interference [38]. This assumption holds more strongly when $T_s \leq \frac{1}{f_D}$. In our simulations, we set the normalized Doppler frequency $f_D T_s \leq 0.03$. The additive noise $\mathbf{N}[t]$ follows an uncorrelated complex Gaussian distribution with zero mean and covariance $\sigma^2 \mathbf{I}_{N_r}$. The reflecting pattern selection procedure is detailed in [40]. While in [40] the receiver is based on CDD, in our present paper we consider DFDD for DRM RIS systems.

The core concept of the DFDD technique involves using previously decoded symbols to feed back and used to establish a demodulation reference assisting the detection of a subsequent symbol. Following the derivation of the DFDD receiver for scalar systems as presented in [37], [38], subsequent research has focused on applying DFDD detection techniques to multi-antenna systems. Notably, two similar formulations for the Differential Space-Time Modulation (DSTM) scheme, which employs decision-feedback differential demodulation, were introduced in [42] and [43]. In [42], it is highlighted that for multi-antenna systems, the scalar predictor coefficients are derived based on the assumption of spatially uncorrelated fading. This assumption ensures that the fading processes are uncorrelated across different spatial paths. In DFDD receivers, the time correlation, however, plays a crucial role. The faster is the fading process, the more performance loss can be expected. In our work, we assume the fading process to be spatially uncorrelated, while the time correlation is dictated by the Doppler spread. In [43] the DFDD technique is extended to a matrix formulation with matrix prediction coefficients $\mathbf{P} = [\mathbf{P}_1, \dots, \mathbf{P}_V]$, where $\mathbf{P}_i = p_i \mathbf{I}$ and V is the prediction order. This matrix coefficient approach is effectively equivalent to using scalar coefficients, maintaining the simplicity and effectiveness of the prediction method.

With the DFDD technique, the receiver uses past decoded symbols to assist in the detection of the current symbol. Using (2), then (3) can be expressed as

$$\mathbf{Y}[t] = \mathbf{H}[t]\mathbf{V}[t-1]\mathbf{X}[t] + \mathbf{N}[t], \quad (4)$$

Using (3) at time instant $t-1$ we have

$$\mathbf{Y}[t-1] = \mathbf{H}[t-1]\mathbf{V}[t-1] + \mathbf{N}[t-1], \quad (5)$$

Since $\mathbf{H}[t] \approx \mathbf{H}[t-1]$ due to the slow variation of the fading process, we have

$$\mathbf{Y}[t] = \mathbf{Y}[t-1]\mathbf{X}[t] + \mathbf{N}[t], \quad (6)$$

if the effect of noise $\mathbf{N}[t-1]$ is neglected. Then, $\mathbf{Y}[t-1]$ can be regarded as an estimate for $\mathbf{H}[t]\mathbf{V}[t-1]$, where the noise terms $\mathbf{N}[t-1]$ induce errors in these estimates. This effect can be reduced by using several past symbols $\mathbf{Y}[t-v]$, and employing a smoothing procedure. The DFDD receiver relies on estimates for $\mathbf{H}[t]\mathbf{V}[t-1]$ in (4) not only from $\mathbf{Y}[t-1]$ but also from the previous observed signals [44]. Optimal linear prediction from previous V signals $\mathbf{Y}[t-v], 1 \leq v \leq V$, for $\mathbf{H}[t]\mathbf{V}[t-1]$ can be interpreted as resulting in a reference signal $\hat{\mathbf{Y}}[t]$ for the detection of $\mathbf{Y}[t]$, and it is formed as [41]

$$\hat{\mathbf{Y}}[t] = \sum_{v=1}^V p_v \mathbf{Y}[t-v] \prod_{\mu=1}^{v-1} \hat{\mathbf{X}}[t-\mu], \quad (7)$$

which it is illustrated in Fig. 2. The product $\prod_{\mu=1}^{v-1} \hat{\mathbf{X}}[t-\mu]$ in Fig. 2 is formed from decision

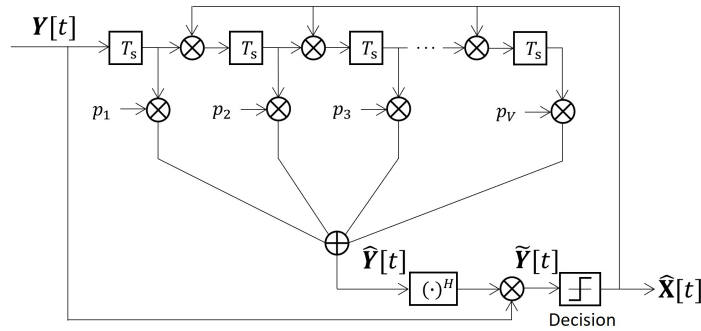


Fig. 2: The structure of a DFDD receiver.

feedback symbols $\hat{\mathbf{X}}[t-(v-1)]$ as

$$\prod_{\mu=1}^{v-1} \hat{\mathbf{X}}[t-\mu] = \begin{cases} \hat{\mathbf{X}}[t-(v-1)] \cdots \hat{\mathbf{X}}[t-1], & v > 1 \\ \mathbf{I}_K, & v = 1 \end{cases} \quad (8)$$

Then, the decision variable for the DFDD receiver is formed as

$$\tilde{\mathbf{Y}}[t] = \hat{\mathbf{Y}}^H[t] \mathbf{Y}[t], \quad (9)$$

and the decision rule is given by [44]

$$\hat{\mathbf{X}}[t] = \arg \max_{\mathbf{X}[t] \in \mathcal{X}} \Re \left[\text{tr} \left(\mathbf{X}[t] \tilde{\mathbf{Y}}^H[t] \right) \right], \quad (10)$$

Using (9) in (10) and (7) we have

$$\begin{aligned}\hat{\mathbf{X}}[t] &= \arg \max_{\mathbf{X}[t] \in \mathcal{X}} \Re \left[\text{tr} \left(\mathbf{X}[t] \mathbf{Y}^H[t] \hat{\mathbf{Y}}[t] \right) \right] \\ &= \arg \max_{\mathbf{X}[t] \in \mathcal{X}} \Re \left[\text{tr} \left(\mathbf{X}[t] \mathbf{Y}^H[t] \sum_{v=1}^V p_v \mathbf{Y}[t-v] \prod_{\mu=1}^{v-1} \hat{\mathbf{X}}[t-\mu] \right) \right],\end{aligned}\quad (11)$$

where V is the prediction order, representing the total number of the previously detected symbols that are used to establish the reference $\hat{\mathbf{Y}}[t]$, and $p_v, v = 1, \dots, V$ are predictor coefficients determined by minimizing the mean-square error (MSE) between $\mathbf{H}[t] \mathbf{V}[t-1]$ and $\hat{\mathbf{Y}}[t]$,

$$\sigma_{\text{mse}}^2 = E \left\{ \left\| \mathbf{H}[t] \mathbf{V}[t-1] - \hat{\mathbf{Y}}[t] \right\|_F^2 \right\}.\quad (12)$$

This criterion ensures that $\hat{\mathbf{Y}}[t]$ is a good approximation to the current channel state $\mathbf{H}[t] \mathbf{V}[t-1]$ when using previous symbol decisions, thereby improving detection performance. In the derivation of predictor coefficients p_v we assume previous decisions are correct as in [37], [38]. The derivation details are presented in Appendix A. It is worth noting that for $V = 1$, (11) is the same as conventional differential detection as long as the predictor coefficients are real.

III. PERFORMANCE OF DFDD-DETECTED DRM

To assess the performance of DFDD in DRM RIS systems we perform extensive Monte-Carlo simulations with BPSK and QPSK modulation. Different scenarios are considered, including various values for $f_D T_s$, and V . In the simulations set up, the SNR is $\rho = \frac{1}{\sigma^2}$, where σ^2 is the variance of each component in the additive noise matrix. For each SNR, we generate $r \cdot 10^9$ information bits, where r is defined in (1). We collect at least 50000-bit errors using Monte Carlo simulations on a space uncorrelated time-varying Rayleigh fading channel based on Jakes' model, where 10^2 blocks of information bits are randomly generated with a discrete uniform distribution, and then transmitted for each frame.

A. Results for $2 \leq K \leq 4$ and BPSK

We start with the error performance of the DFDD receiver for BPSK. To evaluate how different parameters affect the system, in our simulations we vary $f_D T_s$ from 0.01 to 0.03 and change the prediction order V from 1 to 3. Using the system illustrated in Fig. 1, we

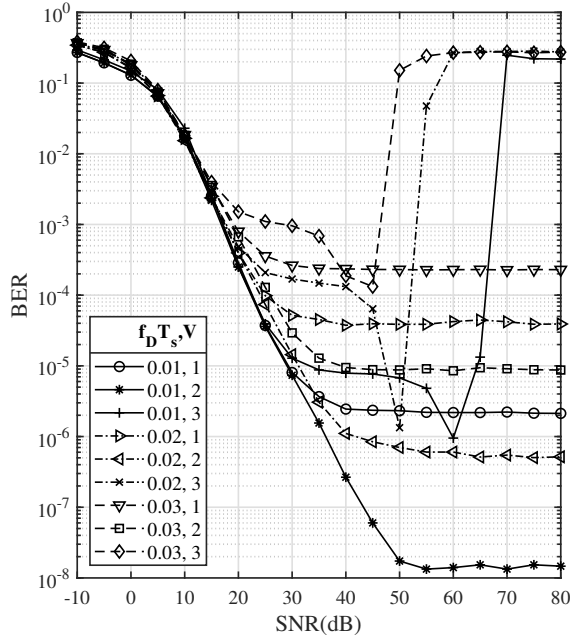


Fig. 3: BER performance of the DFDD-detected DRM system with BPSK when $K = 2$, $f_D T_s = 0.01, 0.02, 0.03$, and $V = 1, 2, 3$.

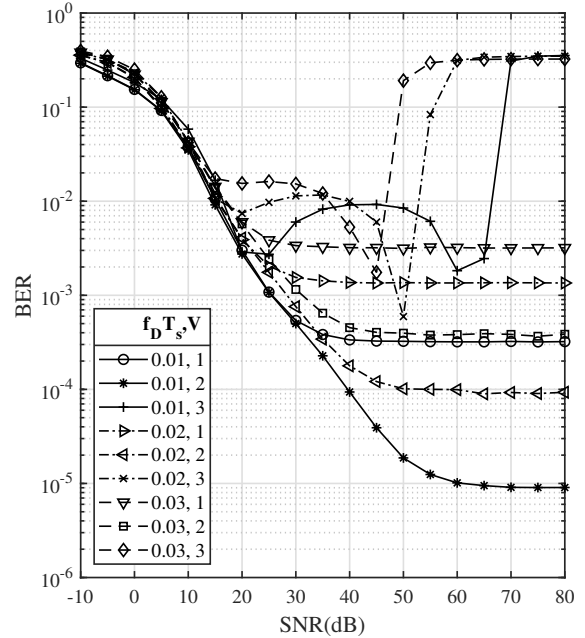


Fig. 4: BER performance of the DFDD-detected DRM system with BPSK when $K = 3$, $f_D T_s = 0.01, 0.02, 0.03$, and $V = 1, 2, 3$.

generate the fading processes using Jakes' model and then proceed with the modulation and perform decoding using the DFDD technique.

In Fig. 3 we present the system performance for $K = 2$. As the normalized Doppler frequency $f_D T_s$ increases from 0.01 to 0.03, there is a noticeable decline in performance across all prediction orders. At a normalized Doppler frequency of 0.01, the system achieves its lowest BER of $2.5 \cdot 10^{-6}$ at an E_b/N_0 of 40 dB with $V = 1$. However, when $f_D T_s$ rises to 0.02, the BER encounters an error floor of approximately $4 \cdot 10^{-5}$ at 35 dB SNR, and at $f_D T_s = 0.03$, the error floor further increases to around $2.4 \cdot 10^{-4}$ at 30 dB SNR. This performance degradation persists for all prediction orders as the normalized Doppler frequency increases. The reason for this is that as $f_D T_s$ grows, the channel varies more rapidly, and hence does not remain the same over past transmitted symbols. The occurrence of an error floor is often attributed to the high error probability associated with the first few decoded symbols. These symbols are decoded by CDD rather than DFDD [45] due to

the insufficient availability of previously decoded symbols for the scheme. However, $V = 2$ provides the lowest error floors. for all values of normalized Doppler, indicating that DFDD has the property of lowering the error floor.

In Fig. 3, for a specific $f_D T_s$, it can be seen that at low SNR, the BER for $V = 2$ is slightly better than for $V = 1$. As the SNR rises, the error performance of $V = 2$ becomes noticeably better than that of $V = 1$. For example, in Fig. 3, when the normalized Doppler frequency is 0.02, the gap between $V = 2$ and $V = 1$ at a BER of 10^{-4} is about 1 dB. As the SNR continues to increase, the BER for $V = 1$ exhibits an error floor around $4 \cdot 10^{-5}$ starting at the SNR of 35 dB. In contrast, the BER for $V = 2$ keeps improving, dropping to 10^{-6} at $E_b/N_0 = 40$ dB. Across all normalized Doppler frequencies, it is evident that $V = 2$ consistently outperforms $V = 1$. The higher prediction order V provides more accurate reference detection symbol (7) improving current symbol detection, and resulting in better performance.

As illustrated in Fig. 3, a larger prediction order may degrade performance. For example, when $f_D T_s = 0.01$ and $V = 3$, the BER reaches a minimum value of 10^{-6} at an E_b/N_0 of 60 dB. However, before this point, the performance is consistently worse compared to that of $V = 1$ and same $f_D T_s$. Then, the error rate rapidly increases in the higher SNR range. For $V = 3$ and $f_D T_s = 0.02$, the BER attains its lowest point at $1.5 \cdot 10^{-6}$ and then sharply increases at E_b/N_0 larger than 50 dB. This phenomenon occurs even earlier for $f_D T_s = 0.03$, with the BER reaching $1.4 \cdot 10^{-4}$ at the SNR of 45 dB. Such trends of BER behaviour can be observed in all scenarios for $V = 3$. With a higher prediction order, the DFDD receiver employs a larger number of previously detected symbols increasing the risk of error propagation. If a previous decision is incorrect, it persist a longer time in the receiver and hence it has a more significant impact in demodulation, possibly resulting in increasing BER. Such a phenomenon for scalar DFDD receivers has been considered in detail in [46]. Therefore for any values of V , performance significantly deteriorates under high Doppler frequencies, making it essential to select an optimal prediction order V for best performance.

Following the performance analysis of the DFDD receiver for $K = 2$, we now consider scenarios where $K \geq 2$ with BPSK. Since increasing K leads to a greater complexity, our evaluations primarily involve $K = 3$ and $K = 4$, of which the BER performance is illustrated in Fig. 4 and Fig. 5, respectively. These figures generally indicate similar error behaviour

as observed for $K = 2$. For a given prediction order V , the system performance worsens as the normalized Doppler frequency increases. For example, when $K = 4$ and $V = 1$, an error floor of $5 \cdot 10^{-4}$ is reached at $E_b/N_0 > 40$ dB for $f_D T_s = 0.01$, while for $f_D T_s = 0.03$, the minimum BER degrades to $5.5 \cdot 10^{-3}$ at $E_b/N_0 > 30$ dB. Across all Doppler frequencies, using $V = 2$ consistently leads to better performance compared to $V = 1$ throughout the SNR range, while larger prediction orders such as $V = 3$ result in performance degradation. For instance, for $K = 3$ and $f_D T_s = 0.01$, $V = 2$ yields a s better performance than $V = 1$ by about 1 dB at a BER of 10^{-3} . With $V = 2$, the BER encounters an error floor of 10^{-5} at an SNR of 60 dB, which is significantly better than the $3.2 \cdot 10^{-4}$ error floor for $V = 1$ at $E_b/N_0 \geq 30$ dB. In contrast, for $f_D T_s = 0.03$ and $V = 3$ in Fig. 4, the BER initially drops to $1.8 \cdot 10^{-3}$ at 45 dB but quickly increases again. Throughout the entire SNR range, $V = 3$ demonstrates worse performance than $V = 2$, with a pronounced difference of 20 dB at a BER of 10^{-2} .

When comparing Fig. 3, Fig. 4, and Fig. 5, with V and $f_D T_s$ constant, it is evident that the error performance deteriorates as K increases,. For example, when $f_D T_s = 0.03$ and $V = 2$, the error floor is approximately $9 \cdot 10^{-6}$ for $K = 2$, $4 \cdot 10^{-4}$ for $K = 3$, and $7 \cdot 10^{-4}$ for $K = 4$. This increase in BER floor as K increases emphasizes the more significant impact of larger K on system performance.

B. Results for DFDD detection with $2 \leq K \leq 4$ and QPSK

We consider now the performance of DFDD receivers in DRM RIS systems with QPSK for $2 \leq K \leq 4$, and compare it to the BPSK case. The normalized Doppler frequency $f_D T_s$ ranges from 0.01 to 0.03, and the prediction order V assumes the values 1, 2 and 3.

As depicted in Figs. 6, 7, and 8, the general behavior with QPSK is similar to that of the BPSK case discussed earlier. A key observation is the rising BER error floor as the Doppler frequency increases, suggesting that QPSK is more sensitive to fast channel variations. For example, in Fig. 6, when $K = 2$ and $V = 1$, for $f_D T_s = 0.01$. the BER reaches an error floor of approximately $2.2 \cdot 10^{-6}$ at $E_b/N_0 \geq 40$ dB. When the Doppler frequency increases to 0.02, the error floor rises to about $5.5 \cdot 10^{-5}$ at SNR values above 30 dB. Additionally, with a prediction order of $V = 2$, the BER performance closely aligns with that of $V = 1$ at lower SNR values. However, as the SNR increases, $V = 2$ presents significantly better performance than $V = 1$. As the SNR increases, $V = 1$ reaches an error floor around $5 \cdot 10^{-5}$

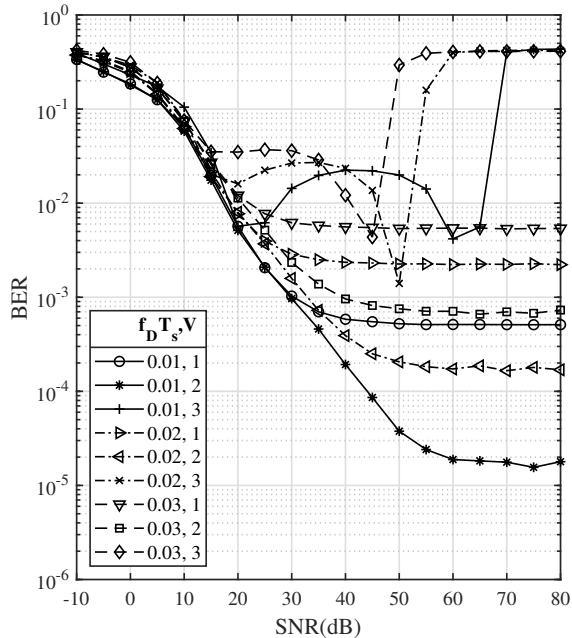


Fig. 5: BER performance of the DFDD-detected DRM system with BPSK when $K = 4$, $f_D T_s = 0.01, 0.02, 0.03$, and $V = 1, 2, 3$.

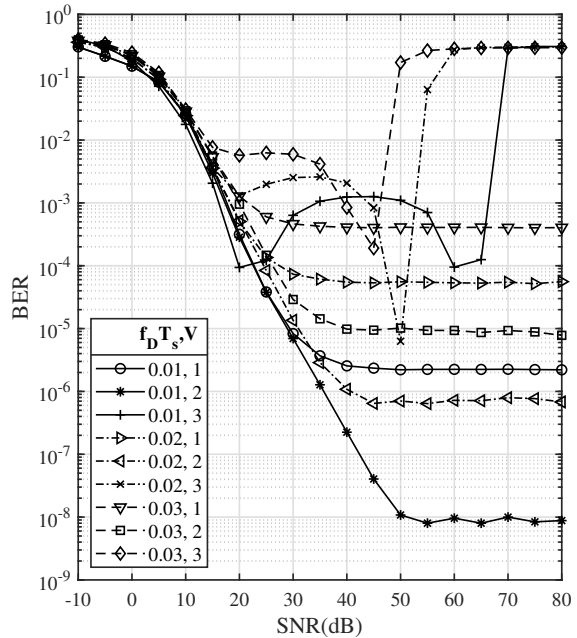


Fig. 6: BER performance of the DFDD-detected DRM system with QPSK when $K = 2$, $f_D T_s = 0.01, 0.02, 0.03$, and $V = 1, 2, 3$.

at $E_b/N_0 \geq 40$ dB, while the BER for $V = 2$ continues to drop, approaching $6 \cdot 10^{-7}$ at the SNR of 45 dB.

The phenomenon of increased BER at high SNR, observed for BPSK appears also for QPSK, especially when the prediction order is 3. As shown in Fig. 8, for $f_D T_s = 0.02$ and $V = 3$, the BER reaches a minimum of $1.5 \cdot 10^{-3}$ at an SNR of 50 dB before rising sharply. Except for this minimum, $V = 3$ consistently performs worse compared to $V = 1$. Moreover, as the Doppler frequency increases, the SNR, at which the BER starts to increase rapidly, decreases. For example, with $f_D T_s = 0.01$ and $V = 3$, the BER attains a minimum of $4 \cdot 10^{-3}$ at $E_b/N_0 = 60$ dB, whereas for $f_D T_s = 0.03$, the minimum BER of $4 \cdot 10^{-3}$ occurs at 45 dB SNR. However, it is seen that also in this case the performance is best when $V = 2$, providing significant advantages over $V = 1$.

We next compare the QPSK performance with the BPSK results presented previously. By comparing Fig. 6 with Fig. 3, it is clear that the error floors for QPSK are approximately the

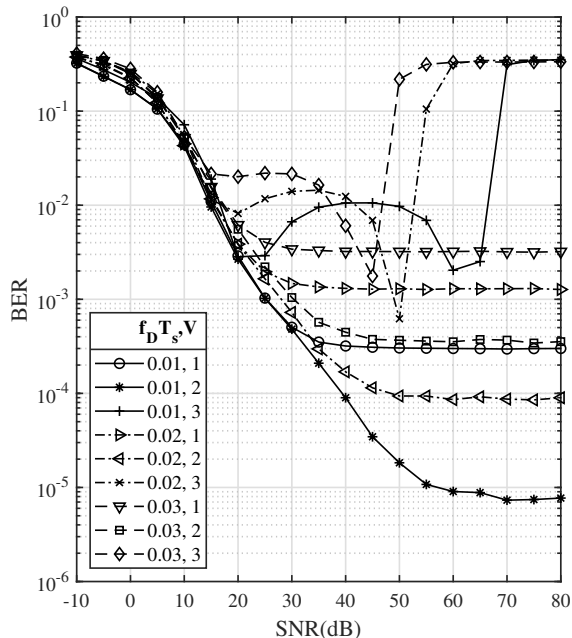


Fig. 7: BER performance of the DFDD-detected DRM system with QPSK when $K = 3$, $f_D T_s = 0.01, 0.02, 0.03$, and $V = 1, 2, 3$.

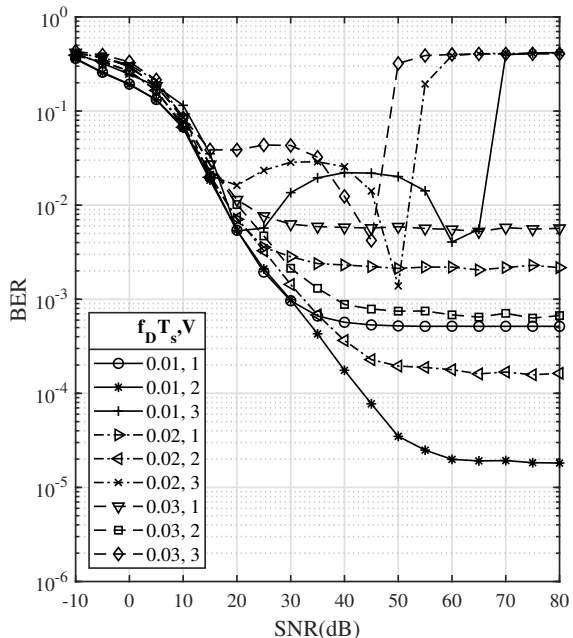


Fig. 8: BER performance of the DFDD-detected DRM system with QPSK when $K = 4$, $f_D T_s = 0.01, 0.02, 0.03$, and $V = 1, 2, 3$.

same or only slightly higher than those for BPSK. When the normalized Doppler frequency is 0.03 and the prediction order is 1, BPSK reaches an error floor at a BER of about $2.3 \cdot 10^{-4}$, while QPSK encounters a slightly higher floor at $4 \cdot 10^{-4}$. However, in most cases, the performance of BPSK and QPSK is quite close, particularly in the high SNR range. This similarity in behavior can also be seen in the DRM schemes over slower fading channels. For example, in Figs. 5 and 8, for a normalized Doppler frequency of 0.01 and a prediction order of $V = 2$, both constellations reach an error floor around $1.8 \cdot 10^{-5}$ at $E_b/N_0 \geq 60$ dB.

To examine the performance when $V = 3$ and $f_D T_s = 0.02$, Fig. 6 shows that with QPSK the lowest BER point, where the BER starts increasing, occurs at around $6 \cdot 10^{-6}$ at $E_b/N_0 = 50$ dB. In comparison, Fig. 3 demonstrates that BPSK achieves a lower minimum BER of approximately $1.5 \cdot 10^{-6}$ at the same E_b/N_0 value, indicating a slight advantage for BPSK over QPSK in this context.

IV. COMPARISON WITH CONVENTIONAL DIFFERENTIAL DETECTION (CDD) OF DRM AND COMPLEXITY ANALYSIS

In this section, we compare the performance of the proposed DFDD-detected DRM scheme with the original DRM system as well as with Differential Space-Time Modulation (DSTM) coded DRM scheme from [40] using CDD. It was shown in [40], that over fading time varying channels, DRM with DSTM can also reduce error floors. Hence from this point of view it is interesting to compare with uncoded DRM with DFDD which was shown to have same property. Then, the complexity of these systems is analyzed.

A. Performance Comparison

Results for uncoded DRM and DRM-DSTM systems from [40], which both use CDD, are compared with DRM with DFDD for $K = 2, 3, 4$ over Jake's fading channels. The notation for DSTM coded DRM follows the same format as in [40]. In this section we select the parameters that provide the best performance at comparable levels of complexity as found in our work. For instance, choosing $V = 2$ for DFDD provides the best performance, particularly at high SNR.

In Fig. 9, 10, and 11 we illustrate the performance of DRM, DRM-DSTM with CDD, and DRM with DFDD, over time varying channels with $f_D T_s = 0.01$. We note a clear performance difference between these three schemes, however in all these cases we see a marked error floor effect. From [40] we have that over quasi-static fading channels, employing suitable cyclic or dicyclic codes in DRM-DSTM significantly enhances performance relative to uncoded DRM. This benefit of DSTM is also evident under time-varying conditions. For example, in Fig. 10, with $K = 3$ and $f_D T_s = 0.01$, the $(4; 1, 1, 1)$ -coded system improves performance by about 6 dB over the uncoded DRM with QPSK at a BER of 10^{-3} . At $E_b/N_0 \geq 30$ dB, the $(2; 1, 1, 1)$ -coded and $(4; 1, 1, 1)$ -coded schemes are impaired by error floors of $2 \cdot 10^{-4}$ and $3 \cdot 10^{-4}$, respectively, whereas the original DRM scheme achieves a minimum BER of $4.2 \cdot 10^{-4}$. This performance gap widens with increasing K , as shown by the approximately 11 dB difference between the $(2; 1, 1, 1, 1)$ coded system and the uncoded BPSK scheme at a BER of 10^{-3} in Fig. 11, compared to a 7 dB gap between the $(2; 1, 1)$ cyclic-coded scheme and the uncoded scheme in Fig. 9.

Furthermore, for $K = 4$, the performance of the cyclic and dicyclic coded systems is nearly identical. For instance, in Fig. 11 with $f_D T_s = 0.01$, the performance difference between

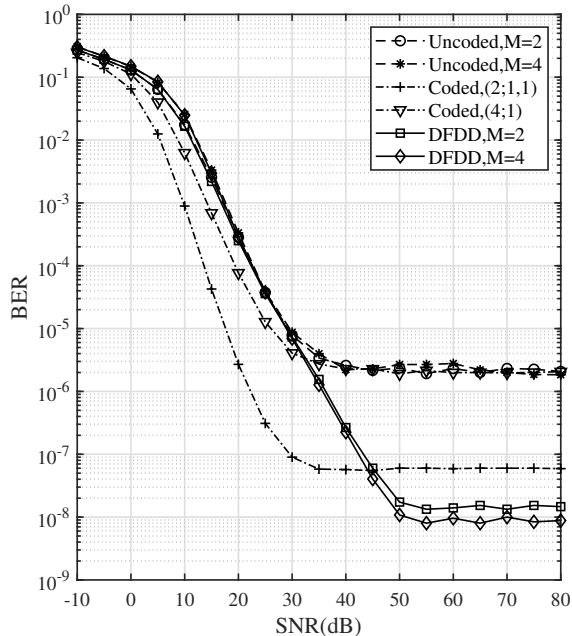


Fig. 9: BER performance of DRM,,
DRM-DSTM with CDD and DRM with
DFDD for $K = 2$. and $f_D T_s = 0.01$

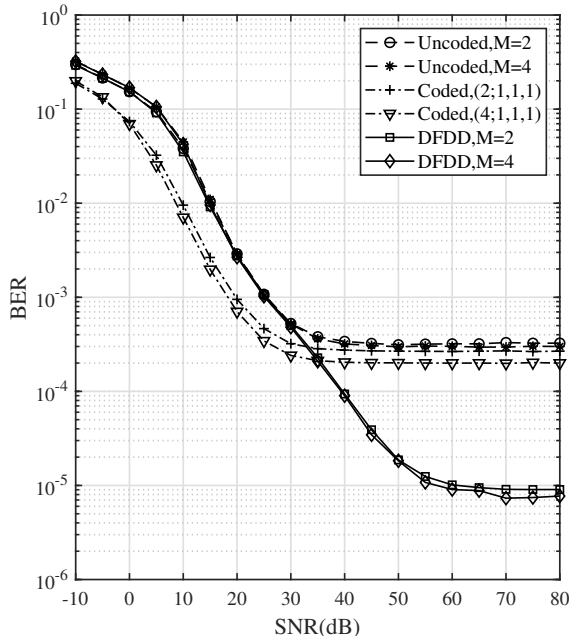


Fig. 10: BER performance of DRM,,
DRM-DSTM with CDD and DRM with
DFDD for $K = 3$. and $f_D T_s = 0.01$

cyclic $(2, 1, 1, 1, 1)$ and dicyclic $(4, 1, 1)$ codes is negligible, with both curves overlapping almost entirely across the SNR range. In contrast, for $K = 2$, Fig. 9 reveals a substantial performance discrepancy between two types of the group codes. Specifically, at a BER of 10^{-5} , the $(2; 1, 1)$ cyclic-coded scheme outperforms the $(4; 1)$ dicyclic-coded scheme by about 8 dB. The $(2; 1, 1)$ -coded scheme reaches an error floor of $5.9 \cdot 10^{-8}$ at $E_b/N_0 \geq 35$ dB, whereas the $(4; 1)$ -coded scheme shows an error floor of $2.5 \cdot 10^{-6}$ for SNR above 35 dB.

Next we compare the performance of the DFDD system with the original DRM with DRM-DSTM schemes. As observed, increasing Doppler frequency generally degrades performance across all SNR ranges. Therefore, we focus on $f_D T_s = 0.01$ for clarity in the figures. It is evident that while DFDD-based DRM schemes initially lag behind DSTM-coded schemes, they eventually surpass them at high SNR levels. Compared to the original DRM schemes, DFDD schemes perform similarly at low SNR but performs better as SNR increases. In Fig. 9, at a BER of 10^{-4} , the DFDD for $f_D T_s = 0.01$ lags approximately by 3.5 dB behind the $(2; 1, 1)$ -coded scheme and shows almost no difference from the uncoded DRM. As SNR

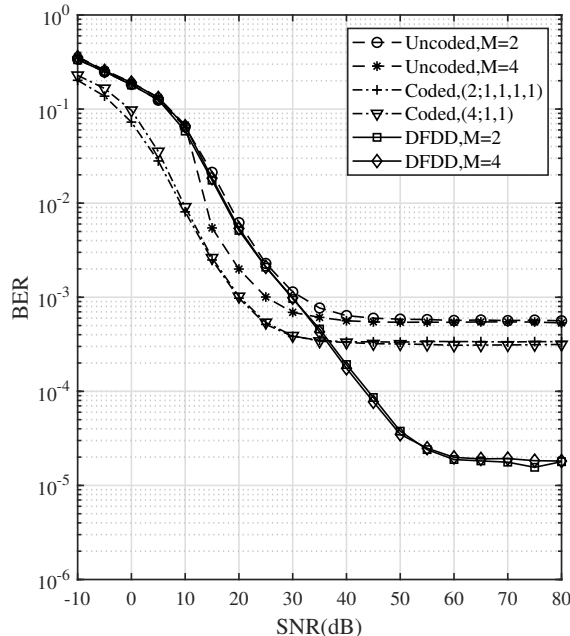


Fig. 11: BER performance of DRM,, DRM-DSTM with CDD and DRM with DFDD for $K = 4.$ and $f_D T_s = 0.01$

risers, this gap grows; for example, at a BER of 10^{-6} , the difference between DFDD and DSTM systems increases to about 11.5 dB. The poorer performance of DFDD at low SNR is attributed to more errors being propagated in the decision feedback process, as discussed in section III-A. However, as SNR increases, the advantages of DFDD systems become more apparent. The CDD-detected DRM scheme reaches an error floor of approximately $2.5 \cdot 10^{-6}$ at $E_b/N_0 \geq 40$ dB, and it falls significantly behind DFDD-detected schemes for both BPSK and QPSK. The BER of the DFDD scheme continues to improve until it reaches an error floor around 10^{-8} . Similarly to DRM with BPSK and QPSK, the DFDD scheme exhibits nearly identical BER performance for both signal constellations at high SNR. In Fig. 9, for instance, the (2; 1, 1)-coded scheme encounters an error floor of $5.7 \cdot 10^{-8}$ at $E_b/N_0 \geq 35$ dB, while the BER of DFDD with uncoded BPSK keeps decreasing, eventually reaching a lower error floor of $1.5 \cdot 10^{-8}$ at 50 dB SNR. The DFDD scheme with uncoded BPSK outperforms the (2; 1, 1)-coded scheme at an SNR of around 45 dB, with a similar crossover occurring earlier for QPSK at an SNR of 32 dB.

These trends are also observed in other figures with different K values. In Fig. 10, both

BPSK and QPSK show that DFDD starts to outperform DRM schemes at $E_b/N_0 \geq 30$ dB, although both systems perform similarly at low SNR. The DFDD scheme, for example, is impaired by an error floor of approximately 10^{-5} , which is significantly lower than the DRM error floor of $4.2 \cdot 10^{-4}$. While the DSTM-coded scheme initially performs better, it is eventually surpassed by the DFDD system at medium to high SNR and reaches a higher error floor compared to DFDD. For instance, the (4; 1, 1, 1)-coded scheme with QPSK shows a 6 dB advantage at a BER of 10^{-3} at low SNR but reaches an error floor of $2 \cdot 10^{-4}$ at $E_b/N_0 \geq 35$ dB, while the BER continues to improve for DFDD, reaching an error floor of $8 \cdot 10^{-6}$ beyond 55 dB.

Despite the overall degradation in error rate performance with increasing K , the trends we discussed before remain the same. For $K = 4$ in Fig. 11, a clear performance gap emerges between DFDD and DRM schemes after $E_b/N_0 = 30$ dB, with the two schemes reaching error floors of approximately $2 \cdot 10^{-5}$ and $5.7 \cdot 10^{-4}$, respectively. The (2; 1, 1, 1, 1) cyclic-coded scheme outperforms DFDD with QPSK by about 10 dB at a BER of 10^{-3} . However, an error floor of $3.7 \cdot 10^{-4}$ at an SNR of 30 dB SNR impairs the coded scheme, while the DFDD scheme eventually achieves an error floor of $2 \cdot 10^{-5}$ at $E_b/N_0 \geq 60$ dB.

B. Complexity Analysis

This section examines the encoding and decoding complexity of the DFDD system, comparing it with the DSTM-coded system and the uncoded DRM scheme both with CDD receivers.

First, the common processes of generating permutation matrices, mapping M -PSK symbols, and obtaining information-carrying matrices, as used in the DRM scheme, are omitted. The differential encoding described in (2) has a time complexity of $O(K^3)$. The number of multiplications involved during modulation in (3) is $K^2 \cdot N_r \cdot K = N_r K^3$, making the overall complexity to be $O(K^3)$. A summary of the time complexity for each encoding step is provided in Table I.

During the detection, following (11), for each candidate $\mathbf{X}[t] \in \mathcal{X}$, $\sum_{v=1}^V ((v-1)K^3 + K^2 N_r) + K^2 N_r + K^3$ multiplications are required for matrices multiplication, resulting in the time complexity being $O(VK^3)$. By iterating over $|\mathcal{X}| = 2^r$ candidates, the time complexity of the whole demodulation process is $O(2^r V K^3)$. The computing of trace includes K additions and the time complexity is $O(K)$.

TABLE I: Time complexity of each step in the encoding process of DFDD-detected DRM scheme

	Multiplication	Addition	Copy	Time Complexity
Generate permutation matrix	-	-	-	$O(\binom{K^1}{2^{r_1}})$
M-PSK symbol mapping	-	-	-	$O(K \log_2 M)$
Generate information-carrying matrix	K^3	-	-	$O(K^3)$
Differential Encoding	K^3	-	-	$O(K^3)$
Generate channel matrix	$K^2 N^2 N_r + K^2 N N_r$	$N_r K$	-	$O(K^2)$
Modulation	$K^2 N_r$	$N_r K$	-	$O(K^2)$

TABLE II: Detector complexity comparison

Detector	Numbers of Multiplications	Time Complexity
Uncoded DRM with CDD	$K^2 N_r + K^3$	$O(2^r K^3)$
DSTM-coded DRM with CDD	$K^2 N_r + K^3$	$O(2^{r'} K^3)$
Uncoded DRM with DFDD	$\sum_{v=1}^V ((v-1)K^3 + K^2 N_r) + K^2 N_r + K^3$	$O(2^r V K^3)$

In conclusion, the main difference in time complexity of the DFDD-detected system with respect to the uncoded DRM scheme and DSTM-coded system with CDD is the detection process. Table II presents the numbers of multiplications required for each system during detection, which indicate the difference between the three schemes. It is seen that the DFDD complexity depends linearly on the predictor order V . The DSTM coded DRM has the largest time complexity due to the term $2^{r'}$.

V. CONCLUSIONS

In this paper, we consider the use of a DFDD technique, not requiring channel state information for detection in DRM RIS systems. The use of CDD, which is more common in such systems, results in performance loss and error floors over time-varying fading channels, while DFDD based receivers address these shortcomings at the expense of a modest increased complexity. In this paper we present a mathematical derivation of the DFDD receiver for the DRM RIS scheme with suitable simplifications. Monte-Carlo simulation results over Jakes' fading channels are used to assess performance. We show that the best performance for DFDD receivers in our RIS systems is obtained when the DFDD prediction order is 2. When comparing DRM with DFDD receivers to DRM employing CDD receivers over time-

varying fading channels, DFDD shows comparable performance at low SNR. However, in the medium SNR range, DFDD continues to improve its error rate, whereas the DRM scheme is impaired by a relatively high error floor. The clear advantage of DFDD receivers for DRM over CDD receivers is the significantly lower error floor over time varying fading channels. Although DRM-DSTM coded schemes with CDD receivers also lower the error floor when compared to uncoded DRM with CDD, this work shows that uncoded DRM with DFDD still has the lowest error floor among the three schemes we considered. The chief merits of the DFDD technique for DRM RIS systems is its significantly lower error floors over fading time varying channels even when the prediction order is 2, as used in our paper. Directions for further research on this subject could be the use of DFDD techniques for coded DRM-DSTM systems. The use of DFDD is a challenging research direction even for scalar channels, however it is envisaged that it could generate useful results. Another future research direction could be to develop alternate designs for the prediction coefficients of DFDD receivers following the approach from [47], which has to be adapted to DRM RIS systems. This can allow the increase of the prediction order beyond 2, reducing the decision feedback error propagation effects, and ultimately improving performance.

APPENDIX A

DERIVATION OF PREDICTOR COEFFICIENTS

In this appendix, we present the derivation of the predictor coefficients p_v from (7). Minimizing (12) is equivalent to minimizing

$$\begin{aligned}\sigma_{\text{mse}}^2 &= E\left\{\left\|\mathbf{H}[t]\mathbf{V}[t-1] - \hat{\mathbf{Y}}[t]\right\|_F^2\right\} = E\left\{\left\|\mathbf{Y}[t]\mathbf{X}^{-1}[t] - \mathbf{N}[t]\mathbf{X}^{-1}[t] - \hat{\mathbf{Y}}[t]\right\|_F^2\right\} \\ &= E\left\{\left\|\mathbf{Y}[t] - \mathbf{N}[t] - \hat{\mathbf{Y}}[t]\mathbf{X}[t]\right\|_F^2\right\}\end{aligned}\quad (13)$$

since (4) can be further expressed as

$$\mathbf{Y}[t] - \mathbf{N}[t] = \mathfrak{H}[t]\mathbf{V}[t-1]\mathbf{X}[t], \quad (14)$$

$$(\mathbf{Y}[t] - \mathbf{N}[t])\mathbf{X}^{-1}[t] = \mathfrak{H}[t]\mathbf{V}[t-1]. \quad (15)$$

In (15), $\mathbf{X}[t]$ is invertible because it is a product of a permutation matrix and a diagonal matrix with diagonal entries taking values over M -PSK constellations. It is known that a permutation matrix is also orthogonal, which is necessarily invertible with $\mathbf{Z}^{-1}[t] = \mathbf{Z}^T[t]$. A diagonal matrix, is invertible as long as its diagonal elements are all nonzero. Its inverse is

another diagonal matrix with reciprocals of the original diagonal entries. As a product of two invertible matrices, $\mathbf{X}[t]$ is invertible as well. Without decision feedback errors, $\hat{\mathbf{X}}[t-v] = \mathbf{X}[t-v]$, $1 \leq v \leq V-1$, yielding

$$\prod_{\mu=1}^{v-1} \hat{\mathbf{X}}[t-\mu] \mathbf{X}[t] = \prod_{\mu=1}^{v-1} \mathbf{X}[t-\mu] \mathbf{X}[t-0] = \prod_{\mu=0}^{v-1} \mathbf{X}[t-\mu]. \quad (16)$$

In addition, we have

$$\begin{aligned} \mathbf{V}[t] &= \mathbf{V}[t-v] \prod_{\mu=0}^{v-1} \mathbf{X}[t-\mu] \\ \mathbf{V}^{-1}[t-v] \mathbf{V}[t] &= \prod_{\mu=0}^{v-1} \mathbf{X}[t-\mu]. \end{aligned} \quad (17)$$

Therefore, (13) can be further expressed as

$$\begin{aligned} \sigma_{\text{mse}}^2 &= E \left\{ \left\| \mathbf{Y}[t] - \mathbf{N}[t] - \hat{\mathbf{Y}}[t] \mathbf{X}[t] \right\|_F^2 \right\} \\ &= E \left\{ \left\| \mathbf{H}[t] \mathbf{V}[t] + \mathbf{N}[t] - \mathbf{N}[t] - \left(\sum_{v=1}^V p_v \mathbf{Y}[t-v] \prod_{\mu=1}^{v-1} \hat{\mathbf{X}}[t-\mu] \right) \mathbf{X}[t] \right\|_F^2 \right\} \\ &= E \left\{ \left\| \mathbf{H}[t] \mathbf{V}[t] - \left[\sum_{v=1}^V p_v \left(\mathbf{H}[t-v] \mathbf{V}[t-v] + \mathbf{N}[t-v] \right) \prod_{\mu=1}^{v-1} \hat{\mathbf{X}}[t-\mu] \right] \mathbf{X}[t] \right\|_F^2 \right\} \\ &= E \left\{ \left\| \mathbf{H}[t] \mathbf{V}[t] - \left[\sum_{v=1}^V p_v \left(\mathbf{H}[t-v] \mathbf{V}[t-v] \prod_{\mu=1}^{v-1} \hat{\mathbf{X}}[t-\mu] + \mathbf{N}[t-v] \prod_{\mu=1}^{v-1} \hat{\mathbf{X}}[t-\mu] \right) \right] \mathbf{X}[t] \right\|_F^2 \right\} \\ &= E \left\{ \left\| \mathbf{H}[t] \mathbf{V}[t] - \left[\sum_{v=1}^V p_v \left(\mathbf{H}[t-v] \mathbf{V}[t-1] + \mathbf{N}[t-v] \prod_{\mu=1}^{v-1} \hat{\mathbf{X}}[t-\mu] \right) \right] \mathbf{X}[t] \right\|_F^2 \right\} \\ &= E \left\{ \left\| \mathbf{H}[t] \mathbf{V}[t] - \left[\sum_{v=1}^V p_v \left(\mathbf{H}[t-v] \mathbf{V}[t-1] \mathbf{X}[t] + \mathbf{N}[t-v] \prod_{\mu=1}^{v-1} \hat{\mathbf{X}}[t-\mu] \mathbf{X}[t] \right) \right] \right\|_F^2 \right\} \\ &= E \left\{ \left\| \mathbf{H}[t] \mathbf{V}[t] - \sum_{v=1}^V p_v \left(\mathbf{H}[t-v] \mathbf{V}[t] + \mathbf{N}[t-v] \prod_{\mu=0}^{v-1} \mathbf{X}[t-\mu] \right) \right\|_F^2 \right\} \\ &= E \left\{ \left\| \mathbf{H}[t] \mathbf{V}[t] - \sum_{v=1}^V p_v \left(\mathbf{H}[t-v] \mathbf{V}[t] + \mathbf{N}[t-v] \mathbf{V}^{-1}[t-v] \mathbf{V}[t] \right) \right\|_F^2 \right\} \\ &= E \left\{ \left\| \mathbf{H}[t] \mathbf{V}[t] - \sum_{v=1}^V p_v \left(\mathbf{H}[t-v] + \mathbf{N}[t-v] \mathbf{V}^{-1}[t-v] \right) \mathbf{V}[t] \right\|_F^2 \right\} \\ &= E \left\{ \left\| \left(\mathbf{H}[t] - \sum_{v=1}^V p_v \left(\mathbf{H}[t-v] + \mathbf{N}[t-v] \mathbf{V}^{-1}[t-v] \right) \right) \left(\mathbf{V}[t] \right) \right\|_F^2 \right\} \\ &= E \left\{ \left\| \mathbf{H}[t] - \sum_{v=1}^V p_v \left(\mathbf{H}[t-v] + \mathbf{N}[t-v] \mathbf{V}^H[t-v] \right) \right\|_F^2 \right\}. \end{aligned} \quad (18)$$

We have $\mathbf{V}[t] = \mathbf{I} \mathbf{X}[1] \mathbf{X}[2] \cdots \mathbf{X}[t]$ from (2). The matrix $\mathbf{X}[t]$ is unitary because it is a product of the unitary matrix $\mathbf{Z}[t]$ and a diagonal matrix $\mathbf{S}[t]$ with diagonal elements

being M -PSK symbols. Hence $\mathbf{Z}^H[t] = \mathbf{Z}^{-1}[t]$ and $\mathbf{S}^H[t]\mathbf{S}[t] = \mathbf{S}[t]\mathbf{S}^H[t] = \mathbf{I}$, $\mathbf{X}^H[t]\mathbf{X}[t] = \mathbf{S}^H[t]\mathbf{Z}^H[t]\mathbf{Z}[t]\mathbf{S}[t] = \mathbf{I} = \mathbf{X}[t]\mathbf{X}^H[t]$. We have $\mathbf{S}^H[t]\mathbf{S}[t] = \mathbf{S}[t]\mathbf{S}^H[t] = \mathbf{I}$ because the product of any M -PSK symbol and its conjugate is 1. Furthermore, the products of unitary matrices are unitary, hence $\mathbf{V}^H[t] = \mathbf{V}^{-1}[t]$, and $\mathbf{V}^H[t]\mathbf{V}[t] = \mathbf{V}[t]\mathbf{V}^H[t] = \mathbf{I}$. The last step follows from the unitary invariance of the Frobenius matrix norm.

The prediction coefficients p_v that minimize σ_{mse}^2 are formally given by

$$p_v = \arg \min_{p_v} E \left\{ \left\| \mathbf{H}[t] - \sum_{v=1}^V p_v \left(\mathbf{H}[t-v] + \mathbf{N}[t-v]\mathbf{V}^H[t-v] \right) \right\|_F^2 \right\} \quad (19)$$

The objective function can be expressed as

$$L = E \left\{ \left\| \mathbf{H}[t] - \sum_{v=1}^V p_v \left(\mathbf{H}[t-v] + \mathbf{N}[t-v]\mathbf{V}^H[t-v] \right) \right\|_F^2 \right\}. \quad (20)$$

Since L is quadratic with respect to p_v , the optimal solution to the minimization problem in (19) is obtained when $\frac{\partial L}{\partial p_v} = 0, v = 1, \dots, mV$, where p_v is complex scalar. The complex derivatives $\frac{\partial L}{\partial p_v}$ are the components of the complex gradient with respect to $p_v, v = 1, \dots, V$. The derivative of a real-value function f with respect to a complex variable x (Wirtinger derivative) is defined as [48], [49]

$$\frac{\partial f(x)}{\partial x} = \frac{1}{2} \left(\frac{\partial f(x)}{\partial \text{Re}(x)} - j \frac{\partial f(x)}{\partial \text{Im}(x)} \right). \quad (21)$$

The derivative of a complex-valued function g with respect to x is defined by

$$\begin{aligned} \frac{\partial g(x)}{\partial x} &= \frac{\partial \text{Re}(g(x))}{\partial x} + j \frac{\partial \text{Im}(g(x))}{\partial x} \\ &= \frac{1}{2} \left(\frac{\partial \text{Re}(g(x))}{\partial \text{Re}(x)} - j \frac{\partial \text{Re}(g(x))}{\partial \text{Im}(x)} \right) + \frac{j}{2} \left(\frac{\partial \text{Im}(g(x))}{\partial \text{Re}(x)} - j \frac{\partial \text{Im}(g(x))}{\partial \text{Im}(x)} \right). \end{aligned} \quad (22)$$

Some results from [49] are used in calculating the complex gradient: $\frac{\partial x}{\partial x} = 1$, $\frac{\partial x}{\partial x^*} = 0$, and $\frac{\partial(x \cdot x^*)}{x} = x^*$, since following (22), and with $x = a + jb$ and a, b being real we have

$$\begin{aligned} \frac{\partial(x \cdot x^*)}{\partial x} &= \frac{\partial(a + bj)(a - bj)}{\partial(a + bj)} = \frac{\partial(a^2 + b^2)}{\partial(a + bj)} \\ &= \frac{1}{2} \left(\frac{\partial(a^2 + b^2)}{\partial a} - j \frac{\partial(a^2 + b^2)}{\partial b} \right) = \frac{1}{2} (2a - j2b) = a - bj = x^*. \end{aligned} \quad (23)$$

If a complex-valued function g does not depend on x^* but only on x , then $\frac{\partial g}{\partial x^*} = 0$ [49].

The complex gradient of L with respect to a complex variable p_v can be expressed as

$$\begin{aligned}
\frac{\partial L}{\partial p_v} &= \frac{\partial E \left\{ \left\| \mathbf{H}[t] - \sum_{v=1}^V p_v \left(\mathbf{H}[t-v] + \mathbf{N}[t-v] \mathbf{V}^H[t-v] \right) \right\|_F^2 \right\}}{\partial p_v} \\
&= \frac{\partial}{\partial p_v} E \left\{ \text{Tr} \left(\mathbf{H}[t] - \sum_{v=1}^V p_v \left(\mathbf{H}[t-v] + \mathbf{N}[t-v] \mathbf{V}^H[t-v] \right) \right) \right. \\
&\quad \left. \left(\mathbf{H}^H[t] - \sum_{v=1}^V p_v^* \left(\mathbf{H}^H[t-v] + \mathbf{V}[t-v] \mathbf{N}^H[t-v] \right) \right) \right\} \\
&= \frac{\partial}{\partial p_v} \left\{ E \left(\text{Tr} \left(\mathbf{H}[t] \mathbf{H}^H[t] \right) \right) - E \left(\text{Tr} \left(\sum_{v=1}^V p_v^* \left(\mathbf{H}[t] \mathbf{H}^H[t-v] + \mathbf{H}[t] \mathbf{V}[t-v] \mathbf{N}^H[t-v] \right) \right) \right) \right. \\
&\quad \left. - E \left(\text{Tr} \left(\sum_{v=1}^V p_v \left(\mathbf{H}[t-v] \mathbf{H}^H[t] + \mathbf{N}[t-v] \mathbf{V}^H[t-v] \mathbf{H}^H[t] \right) \right) \right) \right. \\
&\quad \left. + E \left(\text{Tr} \left(\sum_{v=1}^V p_v \cdot \sum_{v'=1}^V p_{v'}^* \left(\mathbf{H}[t-v] \mathbf{H}^H[t-v'] + \mathbf{H}[t-v] \mathbf{V}[t-v'] \mathbf{N}^H[t-v'] \right. \right. \right. \right. \\
&\quad \left. \left. \left. + \mathbf{N}[t-v] \mathbf{V}^H[t-v] \mathbf{H}^H[t-v'] + \mathbf{N}[t-v] \mathbf{V}^H[t-v] \mathbf{V}[t-v'] \mathbf{N}^H[t-v'] \right) \right) \right) \right\} \quad (24)
\end{aligned}$$

. We have

$$\frac{\partial}{\partial p_v} \left\{ E \left(\text{Tr} \left(\mathbf{H}[t] \mathbf{H}^H[t] \right) \right) \right\} = 0, \quad (25)$$

$$\frac{\partial}{\partial p_v} \left\{ E \left(\text{Tr} \left(\sum_{v=1}^V p_v^* \left(\mathbf{H}[t] \mathbf{H}^H[t-v] + \mathbf{H}[t] \mathbf{V}[t-v] \mathbf{N}^H[t-v] \right) \right) \right) \right\} = 0, \quad (26)$$

since they do not depend on p_v and their derivative with respect to p_v is zero. Hence,

$$\begin{aligned}
\frac{\partial L}{\partial p_v} &= \frac{\partial}{\partial p_v} \left\{ -E \left(\text{Tr} \left(\sum_{v=1}^V p_v \left(\mathbf{H}[t-v] \mathbf{H}^H[t] + \mathbf{N}[t-v] \mathbf{V}^H[t-v] \mathbf{H}^H[t] \right) \right) \right) \right. \\
&\quad + E \left(\text{Tr} \left(\sum_{v=1}^V p_v \cdot \sum_{v'=1}^V p_{v'}^* \left(\mathbf{H}[t-v] \mathbf{H}^H[t-v'] + \mathbf{H}[t-v] \mathbf{V}[t-v'] \mathbf{N}^H[t-v'] \right. \right. \right. \\
&\quad \left. \left. \left. + \mathbf{N}[t-v] \mathbf{V}^H[t-v] \mathbf{H}^H[t-v'] + \mathbf{N}[t-v] \mathbf{V}^H[t-v] \mathbf{V}[t-v'] \mathbf{N}^H[t-v'] \right) \right) \right) \left. \right\} \\
&= -E \left(\text{Tr} \left(\mathbf{H}[t-v] \mathbf{H}^H[t] + \mathbf{N}[t-v] \mathbf{V}^H[t-v] \mathbf{H}^H[t] \right) \right) \\
&\quad + E \left(\text{Tr} \left(\sum_{v'=1}^V p_{v'}^* \left(\mathbf{H}[t-v] \mathbf{H}^H[t-v'] + \mathbf{H}[t-v] \mathbf{V}[t-v'] \mathbf{N}^H[t-v'] \right. \right. \right. \\
&\quad \left. \left. \left. + \mathbf{N}[t-v] \mathbf{V}^H[t-v] \mathbf{H}^H[t-v'] + \mathbf{N}[t-v] \mathbf{V}^H[t-v] \mathbf{V}[t-v'] \mathbf{N}^H[t-v'] \right) \right) \right) \\
&= -E \left(\text{Tr} \left(\mathbf{H}[t-v] \mathbf{H}^H[t] \right) \right) - E \left(\text{Tr} \left(\mathbf{N}[t-v] \mathbf{V}^H[t-v] \mathbf{H}^H[t] \right) \right) \\
&\quad + E \left(\text{Tr} \left(\sum_{v'=1}^V p_{v'}^* \left(\mathbf{H}[t-v] \mathbf{H}^H[t-v'] \right) \right) \right) + E \left(\text{Tr} \left(\sum_{v'=1}^V p_{v'}^* \left(\mathbf{H}[t-v] \mathbf{V}[t-v'] \mathbf{N}^H[t-v'] \right) \right) \right) \\
&\quad + E \left(\text{Tr} \left(\sum_{v'=1}^V p_{v'}^* \left(\mathbf{N}[t-v] \mathbf{V}^H[t-v] \mathbf{H}^H[t-v'] \right) \right) \right) \\
&\quad + E \left(\text{Tr} \left(\sum_{v'=1}^V p_{v'}^* \left(\mathbf{N}[t-v] \mathbf{V}^H[t-v] \mathbf{V}[t-v'] \mathbf{N}^H[t-v'] \right) \right) \right), \tag{27}
\end{aligned}$$

. We have

$$E \left(\text{Tr} \left(\mathbf{N}[t-v] \mathbf{V}^H[t-v] \mathbf{H}^H[t] \right) \right) = \text{Tr} \left(E \left(\mathbf{N}[t-v] \mathbf{V}^H[t-v] \mathbf{H}^H[t] \right) \right) \tag{28}$$

$$= \text{Tr} \left(E \left(\mathbf{N}[t-v] \right) E \left(\mathbf{V}^H[t-v] \right) E \left(\mathbf{H}^H[t] \right) \right) = 0, \tag{29}$$

since the matrix $\mathbf{H}[t]$, the noise matrix $\mathbf{N}[t]$, and the transmitted signal $\mathbf{V}[t]$ are mutually independent, and the fading process and the noise are also spatially uncorrelated. In addition,

$$E \left(\mathbf{N}[t] \right) = \begin{bmatrix} E(n[t]_{11}) & E(n[t]_{12}) & \cdots & E(n[t]_{1K}) \\ E(n[t]_{21}) & E(n[t]_{22}) & \cdots & E(n[t]_{2K}) \\ \vdots & \vdots & \ddots & \vdots \\ E(n[t]_{Nr1}) & E(n[t]_{Nr2}) & \cdots & E(n[t]_{NrK}) \end{bmatrix} = \begin{bmatrix} 0 & 0 & \cdots & 0 \\ 0 & 0 & \cdots & 0 \\ \vdots & \vdots & \ddots & \vdots \\ 0 & 0 & \cdots & 0 \end{bmatrix}. \tag{30}$$

Similarly, we can show

$$E\left(\text{Tr}\left(\sum_{v'=1}^V p_{v'}^* \left(\mathbf{H}[t-v]\mathbf{V}[t-v']\mathbf{N}^H[t-v']\right)\right)\right) = 0, \quad (31)$$

$$E\left(\text{Tr}\left(\sum_{v'=1}^V p_{v'}^* \left(\mathbf{N}[t-v]\mathbf{V}^H[t-v]\mathbf{H}^H[t-v']\right)\right)\right) = 0. \quad (32)$$

Finally, (27) becomes

$$\frac{\partial L}{\partial p_v} = -E\left(\text{Tr}\left(\mathbf{H}[t-v]\mathbf{H}^H[t]\right)\right) + E\left(\text{Tr}\left(\sum_{v'=1}^V p_{v'}^* \left(\mathbf{H}[t-v]\mathbf{H}^H[t-v']\right)\right)\right) \quad (33)$$

$$+E\left(\text{Tr}\left(\sum_{v'=1}^V p_{v'}^* \left(\mathbf{N}[t-v]\mathbf{V}^H[t-v]\mathbf{V}[t-v']\mathbf{N}^H[t-v']\right)\right)\right). \quad (34)$$

To evaluate the first term in (33) we write the resulting matrix in component form

$$\begin{aligned} \mathbf{H}[t-v]\mathbf{H}^H[t] &= \begin{bmatrix} h[t-v]_{11} & h[t-v]_{12} & \cdots & h[t-v]_{1K} \\ h[t-v]_{21} & h[t-v]_{22} & \cdots & h[t-v]_{2K} \\ \vdots & \vdots & \ddots & \vdots \\ h[t-v]_{N_r,1} & h[t-v]_{N_r,2} & \cdots & h[t-v]_{N_r,K} \end{bmatrix} \begin{bmatrix} h^*[t]_{11} & h^*[t]_{21} & \cdots & h^*[t]_{N_r,1} \\ h^*[t]_{12} & h^*[t]_{22} & \cdots & h^*[t]_{N_r,2} \\ \vdots & \vdots & \ddots & \vdots \\ h^*[t]_{1K} & h^*[t]_{2K} & \cdots & h^*[t]_{N_r,K} \end{bmatrix} \\ &= \begin{bmatrix} \sum_{i=1}^K h[t-v]_{1i}h^*[t]_{1i} & \sum_{i=1}^K h[t-v]_{1i}h^*[t]_{2i} & \cdots & \sum_{i=1}^K h[t-v]_{1i}h^*[t]_{N_r,i} \\ \sum_{i=1}^K h[t-v]_{2i}h^*[t]_{1i} & \sum_{i=1}^K h[t-v]_{2i}h^*[t]_{2i} & \cdots & \sum_{i=1}^K h[t-v]_{2i}h^*[t]_{N_r,i} \\ \vdots & \vdots & \ddots & \vdots \\ \sum_{i=1}^K h[t-v]_{N_r,i}h^*[t]_{1i} & \sum_{i=1}^K h[t-v]_{N_r,i}h^*[t]_{2i} & \cdots & \sum_{i=1}^K h[t-v]_{N_r,i}h^*[t]_{N_r,i} \end{bmatrix}. \end{aligned} \quad (35)$$

Since the fading processes are spatially uncorrelated, we have

$$\begin{aligned} &E\left(\text{Tr}\left[\mathbf{H}[t-v]\mathbf{H}^H[t]\right]\right) \\ &= \text{Tr}\left(\begin{bmatrix} \sum_{i=1}^K E(h[t-v]_{1i}h^*[t]_{1i}) & 0 & \cdots & 0 \\ 0 & \sum_{i=1}^K E(h[t-v]_{2i}h^*[t]_{2i}) & \cdots & 0 \\ \vdots & \vdots & \ddots & \vdots \\ 0 & 0 & 0 & \sum_{i=1}^K E(h[t-v]_{N_r,i}h^*[t]_{N_r,i}) \end{bmatrix}\right) \\ &= \text{Tr}\left(\begin{bmatrix} K J_0(2\pi f_D T_s v) & 0 & \cdots & 0 \\ 0 & K J_0(2\pi f_D T_s v) & \cdots & 0 \\ \vdots & \vdots & \ddots & \vdots \\ 0 & 0 & 0 & K J_0(2\pi f_D T_s v) \end{bmatrix}\right) \\ &= N_r K J_0(2\pi f_D T_s v), \end{aligned} \quad (36)$$

Similarly, the second term in (33) can be expressed as

$$\sum_{v'=1}^V p_{v'}^* E \left(\text{Tr} \left[\mathbf{H}[t-v] \mathbf{H}^H[t-v'] \right] \right) = \sum_{v'=1}^V p_{v'}^* N_r K J_0(2\pi f_D T_s(v'-v)). \quad (37)$$

Then, to find the third term, we first derive

$$\begin{aligned} & \mathbf{V}^H[t-v] \mathbf{V}[t-v'] \\ &= \begin{bmatrix} v^*[t-v]_{11} & v^*[t-v]_{21} & \cdots & v^*[t-v]_{K1} \\ v^*[t-v]_{12} & v^*[t-v]_{22} & \cdots & v^*[t-v]_{K2} \\ \vdots & \vdots & \ddots & \vdots \\ v^*[t-v]_{1K} & v^*[t-v]_{2K} & \cdots & v^*[t-v]_{KK} \end{bmatrix} \begin{bmatrix} v[t-v']_{11} & v[t-v']_{12} & \cdots & v[t-v']_{1K} \\ v[t-v']_{21} & v[t-v']_{22} & \cdots & v[t-v']_{2K} \\ \vdots & \vdots & \ddots & \vdots \\ v[t-v']_{K1} & v[t-v']_{K2} & \cdots & v[t-v']_{KK} \end{bmatrix} \\ &= \begin{bmatrix} \sum_{i=1}^K v^*[t-v]_{i1} v[t-v']_{i1} & \sum_{i=1}^K v^*[t-v]_{i1} v[t-v']_{i2} & \cdots & \sum_{i=1}^K v^*[t-v]_{i1} v[t-v']_{iK} \\ \sum_{i=1}^K v^*[t-v]_{i2} v[t-v']_{i1} & \sum_{i=1}^K v^*[t-v]_{i2} v[t-v']_{i2} & \cdots & \sum_{i=1}^K v^*[t-v]_{i2} v[t-v']_{iK} \\ \vdots & \vdots & \ddots & \vdots \\ \sum_{i=1}^K v^*[t-v]_{iK} v[t-v']_{i1} & \sum_{i=1}^K v^*[t-v]_{iK} v[t-v']_{i2} & \cdots & \sum_{i=1}^K v^*[t-v]_{iK} v[t-v']_{iK} \end{bmatrix}. \end{aligned} \quad (38)$$

Next, we have

$$\begin{aligned} & \mathbf{N}[t-v] \mathbf{V}^H[t-v] \mathbf{V}[t-v'] = \begin{bmatrix} n[t-v]_{11} & n[t-v]_{12} & \cdots & n[t-v]_{1K} \\ n[t-v]_{21} & n[t-v]_{22} & \cdots & n[t-v]_{2K} \\ \vdots & \vdots & \ddots & \vdots \\ n[t-v]_{N_r,1} & n[t-v]_{N_r,2} & \cdots & n[t-v]_{N_r,K} \end{bmatrix} \mathbf{V}^H[t-v] \mathbf{V}[t-v'] \\ &= \begin{bmatrix} \sum_{j=1}^K \sum_{i=1}^K n[t-v]_{1j} v^*[t-v]_{ij} v[t-v']_{i1} & \cdots & \sum_{j=1}^K \sum_{i=1}^K n[t-v]_{1j} v^*[t-v]_{ij} v[t-v']_{iK} \\ \vdots & \ddots & \vdots \\ \sum_{j=1}^K \sum_{i=1}^K n[t-v]_{N_r,j} v^*[t-v]_{ij} v[t-v']_{i1} & \cdots & \sum_{j=1}^K \sum_{i=1}^K n[t-v]_{N_r,j} v^*[t-v]_{ij} v[t-v']_{iK} \end{bmatrix}, \end{aligned} \quad (39)$$

where the element at the p -th row and q -th column is $\sum_{j=1}^K \sum_{i=1}^K n[t-v]_{pj} v^*[t-v]_{ij} v[t-v']_{iq}$, $1 \leq p \leq N_r$, $1 \leq q \leq K$. Finally, the resulting matrix of (34) is

$$\begin{aligned} & \mathbf{N}[t-v] \mathbf{V}^H[t-v] \mathbf{V}[t-v'] \mathbf{N}^H[t-v'] \\ &= \mathbf{N}[t-v] \mathbf{V}^H[t-v] \mathbf{V}[t-v'] \begin{bmatrix} n^*[t-v']_{11} & n^*[t-v']_{21} & \cdots & n^*[t-v']_{N_r,1} \\ n^*[t-v']_{12} & n^*[t-v']_{22} & \cdots & n^*[t-v']_{N_r,2} \\ \vdots & \vdots & \ddots & \vdots \\ n^*[t-v']_{1K} & n^*[t-v']_{2K} & \cdots & n^*[t-v']_{N_r,K} \end{bmatrix}. \end{aligned} \quad (40)$$

$$\begin{aligned} & \mathbf{N}[t-v] \mathbf{V}^H[t-v] \mathbf{V}[t-v'] \begin{bmatrix} n^*[t-v']_{11} & n^*[t-v']_{21} & \cdots & n^*[t-v']_{N_r,1} \\ n^*[t-v']_{12} & n^*[t-v']_{22} & \cdots & n^*[t-v']_{N_r,2} \\ \vdots & \vdots & \ddots & \vdots \\ n^*[t-v']_{1K} & n^*[t-v']_{2K} & \cdots & n^*[t-v']_{N_r,K} \end{bmatrix}. \end{aligned} \quad (41)$$

The element at the p -th row and l -th column in (40) where $1 \leq p, l \leq N_r$ is

$$(\mathbf{N}[t-v]\mathbf{V}^H[t-v]\mathbf{V}[t-v']\mathbf{N}^H[t-v'])_{pl} = \sum_{q=1}^K \sum_{j=1}^K \sum_{i=1}^K n[t-v]_{pj} v^*[t-v]_{ij} v[t-v']_{iq} n^*[t-v']_{lq}, \quad (42)$$

Since the noise process is spatially uncorrelated, the expectation of (40) has nonzero values only on its diagonal, and $E(n[t-v]_{pj} n^*[t-v']_{pq})$ is nonzero if and only if $j = q$ and $v = v'$.

Thus, we can express the expectation of the p -th diagonal element in (40) as

$$\begin{aligned} E((\mathbf{N}[t-v]\mathbf{V}^H[t-v]\mathbf{V}[t-v']\mathbf{N}^H[t-v'])_{pp}) &= E\left(\sum_{q=1}^K \sum_{j=1}^K \sum_{i=1}^K n[t-v]_{pj} v^*[t-v]_{ij} v[t-v']_{iq} n^*[t-v']_{pq}\right) \\ &= E\left(\sum_{j=1}^K \sum_{i=1}^K n[t-v]_{pj} v^*[t-v]_{ij} v[t-v']_{ij} n^*[t-v']_{pj}\right) = \sum_{j=1}^K \sum_{i=1}^K E(n[t-v]_{pj} v^*[t-v]_{ij} v[t-v']_{ij} n^*[t-v']_{pj}). \end{aligned} \quad (43)$$

When $v \neq v'$, it is known that the noise processes at different time indices are independent of each other as well as independent of the transmitted signal. Therefore, the expectation of the product of these independent random process is

$$E(n[t-v]_{pj} v^*[t-v]_{ij} v[t-v']_{ij} n^*[t-v']_{pj}) = E(n[t-v]_{pj}) E(v^*[t-v]_{ij} v[t-v']_{ij}) E(n^*[t-v']_{pj}) = 0, \quad (44)$$

since the noise process has zero mean. Then, when $v = v'$, (43) can be written by

$$\begin{aligned} E((\mathbf{N}[t-v]\mathbf{V}^H[t-v]\mathbf{V}[t-v]\mathbf{N}^H[t-v])_{pp}) &= \sum_{j=1}^K \sum_{i=1}^K E(n[t-v]_{pj} v^*[t-v]_{ij} v[t-v]_{ij} n^*[t-v]_{pj}) \\ &= \sum_{j=1}^K E(n[t-v]_{pj} n^*[t-v]_{pj}) \sum_{i=1}^K v^*[t-v]_{ij} v[t-v]_{ij} = \sum_{j=1}^K E(n[t-v]_{pj} n^*[t-v]_{pj}) = \sum_{j=1}^K \sigma^2 = K\sigma^2, \end{aligned} \quad (45)$$

where $\sum_{i=1}^K v^*[t]_{ij} v[t]_{ij} = 1$ for a unitary matrix $\mathbf{V}[t] \in \mathbb{C}^{K \times K}$, because

$$\begin{aligned} \mathbf{I} = \mathbf{V}^H[t]\mathbf{V}[t] &= \begin{bmatrix} v^*[t]_{11} & v^*[t]_{21} & \cdots & v^*[t]_{K1} \\ v^*[t]_{12} & v^*[t]_{22} & \cdots & v^*[t]_{K2} \\ \vdots & \vdots & \ddots & \vdots \\ v^*[t]_{1K} & v^*[t]_{2K} & \cdots & v^*[t]_{KK} \end{bmatrix} \begin{bmatrix} v[t]_{11} & v[t]_{12} & \cdots & v[t]_{1K} \\ v[t]_{21} & v[t]_{22} & \cdots & v[t]_{2K} \\ \vdots & \vdots & \ddots & \vdots \\ v[t]_{K1} & v[t]_{K2} & \cdots & v[t]_{KK} \end{bmatrix} \\ &= \begin{bmatrix} \sum_{i=1}^K v^*[t]_{i1} v[t]_{i1} & 0 & \cdots & 0 \\ 0 & \sum_{i=1}^K v^*[t]_{i2} v[t]_{i2} & \cdots & 0 \\ \vdots & \vdots & \ddots & \vdots \\ 0 & 0 & \cdots & \sum_{i=1}^K v^*[t]_{iK} v[t]_{iK} \end{bmatrix}. \end{aligned} \quad (46)$$

Thus, the general expression of (43) is

$$E((\mathbf{N}[t-v]\mathbf{V}^H[t-v]\mathbf{V}[t-v']\mathbf{N}^H[t-v']))_{pp} = K\sigma^2\delta[v'-v], \quad (47)$$

where $\delta[m] = 1$ only if $m = 0$ and zero otherwise. As a result, (34) is

$$\begin{aligned} \sum_{v'=1}^V p_{v'}^* E\left(\text{Tr}\left[\mathbf{N}[t-v]\mathbf{V}^H[t-v]\mathbf{V}[t-v']\mathbf{N}^H[t-v']\right]\right) &= \sum_{v'=1}^V p_{v'}^* \text{Tr}\left(\begin{bmatrix} K\sigma^2\delta[v'-v] & \cdots & 0 \\ \vdots & \ddots & \vdots \\ 0 & \cdots & K\sigma^2\delta[v'-v] \end{bmatrix}\right) \\ &= \sum_{v'=1}^V p_{v'}^* N_r K\sigma^2\delta[v'-v]. \end{aligned} \quad (48)$$

By setting $\frac{\partial L}{\partial p_v} = 0$ in (33) and (34), we can get

$$\begin{aligned} 0 = \frac{\partial L}{\partial p_v} &= -E\left(\text{Tr}\left(\mathbf{H}[t-v]\mathbf{H}^H[t]\right)\right) + E\left(\text{Tr}\left(\sum_{v'=1}^V p_{v'}^* \left(\mathbf{H}[t-v]\mathbf{H}^H[t-v']\right)\right)\right) \\ &\quad + E\left(\text{Tr}\left(\sum_{v'=1}^V p_{v'}^* \left(\mathbf{N}[t-v]\mathbf{V}^H[t-v]\mathbf{V}[t-v']\mathbf{N}^H[t-v']\right)\right)\right), \end{aligned} \quad (49)$$

which results in

$$\begin{aligned} E\left(\text{Tr}\left(\sum_{v'=1}^V p_{v'}^* \left(\mathbf{H}[t-v]\mathbf{H}^H[t-v']\right)\right)\right) + E\left(\text{Tr}\left(\sum_{v'=1}^V p_{v'}^* \left(\mathbf{N}[t-v]\mathbf{V}^H[t-v]\mathbf{V}[t-v']\mathbf{N}^H[t-v']\right)\right)\right) \\ = E\left(\text{Tr}\left(\mathbf{H}[t-v]\mathbf{H}^H[t]\right)\right). \end{aligned} \quad (50)$$

Then, from (36), (37), and (48), we have

$$\begin{aligned} \sum_{v'=1}^V p_{v'}^* \left(N_r K J_0(2\pi f_D T_s(v'-v))\right) + \sum_{v'=1}^V p_{v'}^* \left(N_r K \sigma^2 \delta[v'-v]\right) &= N_r K J_0(2\pi f_D T_s v) \\ \sum_{v'=1}^V p_{v'}^* \left(J_0(2\pi f_D T_s(v'-v)) + \sigma^2 \delta[v'-v]\right) &= J_0(2\pi f_D T_s v), 1 \leq v \leq V. \end{aligned} \quad (51)$$

To solve (51), we convert the equations into matrix form. We define a matrix $\mathbf{R} \in \mathbb{C}^{V \times V}$ and a vector $\mathbf{b} \in \mathbb{C}^{V \times 1}$ as

$$\mathbf{R} = \begin{bmatrix} J_0(0) + \sigma^2 & J_0(2\pi f_D T_s) & \cdots & J_0(2\pi f_D T_s(V-1)) \\ J_0(-2\pi f_D T_s) & J_0(0) + \sigma^2 & \cdots & J_0(2\pi f_D T_s(V-2)) \\ \vdots & \vdots & \ddots & \vdots \\ J_0(2\pi f_D T_s(1-V)) & J_0(2\pi f_D T_s(2-V)) & \cdots & J_0(0) + \sigma^2 \end{bmatrix}, \quad (52)$$

$$\mathbf{b} = \left[J_0(2\pi f_D T_s) \quad J_0(2\pi f_D T_s \cdot 2) \quad \cdots \quad J_0(2\pi f_D T_s V) \right]^T. \quad (53)$$

It is clear that the element at the v -th row and v' -th column of \mathbf{R} is $\mathbf{R}_{vv'} = J_0(2\pi f_D T_s(v' - v)) + K\sigma^2\delta[v' - v]$ and the v -th element in \mathbf{b} is $\mathbf{b}_v = J_0(2\pi f_D T_s v)$. Thus, (51) becomes

$$\mathbf{R}\mathbf{p} = \mathbf{b}, \quad (54)$$

where $\mathbf{p} = [p_1 \ p_2 \ \cdots \ p_V]^H$, with solution

$$\mathbf{p} = \mathbf{R}^{-1}\mathbf{b}. \quad (55)$$

To prove (54), The left hand side is first expressed in component form as

$$\begin{aligned} \mathbf{R}\mathbf{p} &= \begin{bmatrix} J_0(2\pi f_D T_s(1-1)) + \sigma^2 & J_0(2\pi f_D T_s(2-1)) & \cdots & J_0(2\pi f_D T_s(V-1)) \\ J_0(2\pi f_D T_s(1-2)) & J_0(2\pi f_D T_s(2-2)) + \sigma^2 & \cdots & J_0(2\pi f_D T_s(V-2)) \\ \vdots & \vdots & \ddots & \vdots \\ J_0(2\pi f_D T_s(1-V)) & J_0(2\pi f_D T_s(2-V)) & \cdots & J_0(2\pi f_D T_s(V-V)) + \sigma^2 \end{bmatrix} \begin{bmatrix} p_1^* \\ p_2^* \\ \vdots \\ p_V^* \end{bmatrix} \\ &= \begin{bmatrix} \sum_{v'=1}^V p_{v'}^* (J_0(2\pi f_D T_s(v'-1)) + \sigma^2\delta[v'-1]) \\ \sum_{v'=1}^V p_{v'}^* (J_0(2\pi f_D T_s(v'-2)) + \sigma^2\delta[v'-2]) \\ \vdots \\ \sum_{v'=1}^V p_{v'}^* (J_0(2\pi f_D T_s(v'-V)) + \sigma^2\delta[v'-V]) \end{bmatrix}, \end{aligned} \quad (56)$$

and the right hand side is \mathbf{b} of (53). Therefore, we have

$$\begin{bmatrix} \sum_{v'=1}^V p_{v'}^* (J_0(2\pi f_D T_s(v'-1)) + \sigma^2\delta[v'-1]) \\ \sum_{v'=1}^V p_{v'}^* (J_0(2\pi f_D T_s(v'-2)) + \sigma^2\delta[v'-2]) \\ \vdots \\ \sum_{v'=1}^V p_{v'}^* (J_0(2\pi f_D T_s(v'-V)) + \sigma^2\delta[v'-V]) \end{bmatrix} = \begin{bmatrix} J_0(2\pi f_D T_s \cdot 1) \\ J_0(2\pi f_D T_s \cdot 2) \\ \cdots \\ J_0(2\pi f_D T_s \cdot V) \end{bmatrix}, \quad (57)$$

which corresponds to (51) for $v = 1, \dots, V$.

REFERENCES

- [1] A. Umer, I. Mürsepp, M. M. Alam, and H. Wymeersch, "Reconfigurable intelligent surfaces in 6G radio localization: A survey of recent developments, opportunities, and challenges," *IEEE Communications Surveys & Tutorials*, vol. 27, no. 6, pp. 3526–3560, 2025.
- [2] E. Shi, J. Zhang, H. Du, B. Ai, C. Yuen, D. Niyato, K. B. Letaief, and X. Shen, "RIS-aided cell-free massive MIMO systems for 6G: Fundamentals, system design, and applications," *Proceedings of the IEEE*, vol. 112, no. 4, pp. 331–364, 2024.
- [3] M. Fu, L. Zhu, and R. Zhang, "Multi-IRS enhanced wireless coverage: Deployment optimization based on large-scale channel knowledge," *IEEE Transactions on Wireless Communications*, 2025.
- [4] Q. Wu, Q. Peng, Z. Zhang, X. Shao, Y. Liu, Y. Jiang, Y. Zhao, Y. Zhu, Y. Chen, Z. Ren, *et al.*, "Intelligent reflecting surfaces for integrated sensing and communications: From system coexistence to networked mutualism," *IEEE Communications Surveys & Tutorials*, 2026.

- [5] C. Huang, A. Zappone, G. C. Alexandropoulos, M. Debbah, and C. Yuen, "Reconfigurable Intelligent Surfaces for Energy Efficiency in Wireless Communication," *IEEE Transactions on Wireless Communications*, vol. 18, no. 8, pp. 4157–4170, 2019.
- [6] M. D. Renzo, M. Debbah, D.-T. Phan-Huy, A. Zappone, M.-S. Alouini, C. Yuen, V. Sciancalepore, G. C. Alexandropoulos, J. Hoydis, H. Gacanin, *et al.*, "Smart radio environments empowered by reconfigurable AI meta-surfaces: An idea whose time has come," *EURASIP Journal on Wireless Communications and Networking*, vol. 2019, no. 1, pp. 1–20, 2019.
- [7] M. Di Renzo, K. Ntontin, J. Song, F. H. Danufane, X. Qian, F. Lazarakis, J. De Rosny, D.-T. Phan-Huy, O. Simeone, R. Zhang, *et al.*, "Reconfigurable intelligent surfaces vs. relaying: Differences, similarities, and performance comparison," *IEEE Open Journal of the Communications Society*, vol. 1, pp. 798–807, 2020.
- [8] M. Di Renzo, A. Zappone, M. Debbah, M.-S. Alouini, C. Yuen, J. de Rosny, and S. Tretyakov, "Smart Radio Environments Empowered by Reconfigurable Intelligent Surfaces: How It Works, State of Research, and The Road Ahead," *IEEE Journal on Selected Areas in Communications*, vol. 38, no. 11, pp. 2450–2525, 2020.
- [9] M. Yue, Y. Peng, A.-H. Fawaz, and J. Lee, "Hybrid RIS-Assisted Receive Generalized Space Shift Keying for Wireless Communication," *IEEE Transactions on Vehicular Technology*, 2026.
- [10] M. Yue, Y. Peng, R. Ye, J. Lee, F. Al-Hazemi, and R. Boutaba, "RIS-Assisted Joint Transmitter-Receiver Space Shift Keying Design for Highly Flexible Wireless Communications," *IEEE Transactions on Vehicular Technology*, 2026.
- [11] B. Zhang, L. Mei, K. C. Teh, and E. Basar, "RIS-Aided OTFS With Index Modulation: Performance Analysis and Phase Optimization," *IEEE Transactions on Wireless Communications*, vol. 25, pp. 16245–16258, 2026.
- [12] E. Basar, "Reconfigurable intelligent surface-based index modulation: A new beyond MIMO paradigm for 6G," *IEEE Transactions on Communications*, vol. 68, no. 5, pp. 3187–3196, 2020.
- [13] E. Basar, M. Di Renzo, J. De Rosny, M. Debbah, M.-S. Alouini, and R. Zhang, "Wireless communications through reconfigurable intelligent surfaces," *IEEE Access*, vol. 7, pp. 116753–116773, 2019.
- [14] S. Guo, S. Lv, H. Zhang, J. Ye, and P. Zhang, "Reflecting Modulation," *IEEE Journal on Selected Areas in Communications*, vol. 38, no. 11, pp. 2548–2561, 2020.
- [15] H. Alwazani, A. Kammoun, A. Chaaban, M. Debbah, M.-S. Alouini, *et al.*, "Intelligent reflecting surface-assisted multi-user MISO communication: Channel estimation and beamforming design," *IEEE Open Journal of the Communications Society*, vol. 1, pp. 661–680, 2020.
- [16] R. Wang, S. Zhang, B. Clerckx, and L. Liu, "Low-overhead channel estimation framework for beyond diagonal reconfigurable intelligent surface assisted multi-user MIMO communication," *IEEE Transactions on Signal Processing*, vol. 73, pp. 4700–4717, 2025.
- [17] A. L. de Almeida, B. Sokal, H. Li, and B. Clerckx, "Channel estimation for beyond diagonal RIS via tensor decomposition," *IEEE Transactions on Signal Processing*, 2025.
- [18] L. Zhuo, C. Pan, H. Ren, R. Weng, S. Jin, A. L. Swindlehurst, and J. Wang, "Channel Estimation for RIS-Aided MU-MIMO mmWave Systems With Practical Hybrid Architecture," *IEEE Transactions on Signal Processing*, vol. 73, pp. 5213–5228, 2025.
- [19] P. Zheng, S. Tarboush, H. Sardeddeen, and T. Y. Al-Naffouri, "Mutual coupling-aware channel estimation and beamforming for RIS-assisted communications," *IEEE Transactions on Wireless Communications*, 2025.
- [20] Y. Chen, Z. Ren, J. Xu, and R. Zhang, "Environment-aware IRS deployment via channel knowledge map: Joint sensing-communications coverage optimization," *IEEE Transactions on Network Science and Engineering*, 2026.

- [21] Y. Gao, Z. Lu, X. Wu, W. Yu, S. Liu, J. Du, Y. Jin, S. Zhang, X. Chu, and S. Xu, "AI-Driven Channel State Information (CSI) Extrapolation for 6G: Current Situations, Challenges, and Future Research," *IEEE Communications Surveys and Tutorials*, vol. 28, pp. 4485–4518, 2026.
- [22] Y. Yang, B. Zheng, S. Zhang, and R. Zhang, "Intelligent reflecting surface meets OFDM: Protocol design and rate maximization," *IEEE Transactions on Communications*, vol. 68, no. 7, pp. 4522–4535, 2020.
- [23] L. Wei, C. Huang, G. C. Alexandropoulos, and C. Yuen, "Parallel Factor Decomposition Channel Estimation in RIS-Assisted Multi-User MISO Communication," in *2020 IEEE 11th Sensor Array and Multichannel Signal Processing Workshop (SAM)*, pp. 1–5, 2020.
- [24] Q.-U.-A. Nadeem, A. Kammoun, A. Chaaban, M. Debbah, and M.-S. Alouini, "Asymptotic Max-Min SINR Analysis of Reconfigurable Intelligent Surface Assisted MISO Systems," *IEEE Transactions on Wireless Communications*, vol. 19, no. 12, pp. 7748–7764, 2020.
- [25] Q.-U.-A. Nadeem, H. Alwazani, A. Kammoun, A. Chaaban, M. Debbah, and M.-S. Alouini, "Intelligent Reflecting Surface-Assisted Multi-User MISO Communication: Channel Estimation and Beamforming Design," *IEEE Open Journal of the Communications Society*, vol. 1, pp. 661–680, 2020.
- [26] M. Chowdhury, A. Manolakos, and A. Goldsmith, "Scaling Laws for Noncoherent Energy-Based Communications in the SIMO MAC," *IEEE Transactions on Information Theory*, vol. 62, no. 4, pp. 1980–1992, 2016.
- [27] S. Mishra, S. P. Dash, and G. C. Alexandropoulos, "SER-Optimized Multi-Level ASK Modulations for RIS-Assisted Communications with Energy-and Sign-Based Noncoherent Reception," *IEEE Transactions on Green Communications and Networking*, 2025.
- [28] X. Cai, C. Huang, P. Chen, E. Basar, and C. Yuen, "Design of non-coherent RIS-empowered DCSK with two-level nested index modulation," *IEEE Transactions on Wireless Communications*, vol. 24, no. 4, pp. 3044–3058, 2025.
- [29] X. Cai, C. Huang, E. Basar, W. Xu, L. Wang, M. D. Renzo, and C. Yuen, "Toward RIS-Aided Non-Coherent Communications: A Joint Index Keying M-ary Differential Chaos Shift Keying System," *IEEE Transactions on Wireless Communications*, vol. 22, no. 12, pp. 9045–9062, 2023.
- [30] K. Chen-Hu, G. Alexandropoulos, and A. G. Armada, "Non-coherent modulation with random phase configurations in RIS-empowered cellular MIMO systems," *ITU J Future Evolving Technol*, vol. 3, pp. 374–387, 2022.
- [31] X. Cai, C. Huang, J. An, W. Xu, L. Wang, and C. Yuen, "Non-Coherent Chaotic Communications Aided by RIS: A Performance-Enhanced Approach," *IEEE Communications Letters*, vol. 27, no. 6, pp. 1614–1618, 2023.
- [32] H. Ma, Y. Fang, P. Chen, and Y. Li, "Reconfigurable Intelligent Surface-Aided M -Ary FM-DCSK System: A New Design for Noncoherent Chaos-Based Communication," *IEEE Transactions on Vehicular Technology*, vol. 72, no. 4, pp. 4829–4843, 2023.
- [33] P. Zhang, X. Jin, C. Wan, S. Xing, C. Huang, M. Wen, and Y. Yao, "Rectangular Differential Reflecting Spatial Modulation: A Noncoherent Joint Index-Modulation of RIS-assisted MIMO System," *IEEE Transactions on Communications*, pp. 1–1, 2024.
- [34] S. Guo, J. Ye, P. Zhang, H. Zhang, and M.-S. Alouini, "Differential Reflecting Modulation for Reconfigurable Intelligent Surface-Based Communications," *IEEE Communications Letters*, vol. 25, no. 3, pp. 907–910, 2021.
- [35] H. Leib and S. Pasupathy, "The phase of a vector perturbed by Gaussian noise and differentially coherent receivers," *IEEE Transactions on Information Theory*, vol. 34, no. 6, pp. 1491–1501, 1988.
- [36] F. Edbauer, "Bit error rate of binary and quaternary DPSK signals with multiple differential feedback detection," *IEEE Transactions on Communications*, vol. 40, no. 3, pp. 457–460, 1992.

- [37] R. Schober, W. Gerstacker, and J. Huber, "Decision-feedback differential detection of MDPSK for flat Rayleigh fading channels," *IEEE Transactions on Communications*, vol. 47, no. 7, pp. 1025–1035, 1999.
- [38] R. Schober and W. Gerstacker, "Decision-feedback differential detection based on linear prediction for MDPSK signals transmitted over Ricean fading channels," *IEEE Journal on Selected Areas in Communications*, vol. 18, no. 3, pp. 391–402, 2000.
- [39] V. Pauli and L. Lampe, "Tree-Search Multiple-Symbol Differential Decoding for Unitary Space-Time Modulation," *IEEE Transactions on Communications*, vol. 55, no. 8, pp. 1567–1576, 2007.
- [40] J. Qiu and H. Leib, "Space-time Coded Differential Modulation for Reconfigurable Intelligent Surfaces," *IEEE Open Journal of the Communications Society*, vol. 7, pp. 2287–2305, 2026.
- [41] C. Ling, K. Li, and A. Kot, "On decision-feedback detection of differential space-time modulation in continuous fading," *IEEE Transactions on Communications*, vol. 52, no. 10, pp. 1613–1617, 2004.
- [42] C. Xu, J. Zhang, T. Bai, P. Botsinis, R. G. Maunder, R. Zhang, and L. Hanzo, "Adaptive Coherent/Non-Coherent Single/Multiple-Antenna Aided Channel Coded Ground-to-Air Aeronautical Communication," *IEEE Transactions on Communications*, vol. 67, no. 2, pp. 1099–1116, 2019.
- [43] L.-J. Lampe and R. Schober, "Bit-interleaved coded differential space-time modulation," *IEEE Transactions on Communications*, vol. 50, no. 9, pp. 1429–1439, 2002.
- [44] J. Qiu, "Space-time coded differential modulation and decision feedback differential detection for reconfigurable intelligent surfaces," master's thesis, McGill University, December 2024.
- [45] J. Zhang, "Selective decode-and-forward bidirectional multi-relay networks with regularized weighted decision feedback differential coherent receivers," master's thesis, McGill University, July 2017.
- [46] J. Zhang and H. Leib, "Regularized WDFDC Receivers for Selective Detect-and-Forward Multi-Relaying Systems," *IEEE Open Journal of Vehicular Technology*, vol. 1, pp. 130–145, 2020.
- [47] J. Zhang and H. Leib, "Regularized WDFDC receivers for selective detect-and-forward multi-relaying systems," *IEEE Open Journal of Vehicular Technology*, vol. 1, pp. 130–145, 2020.
- [48] D. Palomar and S. Verdu, "Gradient of mutual information in linear vector Gaussian channels," *IEEE Transactions on Information Theory*, vol. 52, no. 1, pp. 141–154, 2006.
- [49] D. H. Brandwood, "A complex gradient operator and its application in adaptive array theory," in *IEE Proceedings H (Microwaves, Optics and Antennas)*, vol. 130, pp. 11–16, IET Digital Library, 1983.